High-spin structures in the ^{139}Pr nucleus

E. Y. Yeoh (杨韵颐),[1] S. J. Zhu (朱胜江),[1,*] J. G. Wang (王建国),[1,2] Z. G. Xiao (肖志刚),[1] M. Zhang (张明),[1] W. H. Yan (闫威华),[1] R. S. Wang (王仁生),[1] Q. Xu (徐强),[1] X. G. Wu (吴晓光),[3] C. Y. He (贺创业),[3] G. S. Li (李广生),[3] Y. Zheng (郑云),[3] C. B. Li (李聪博),[3] X. P. Cao (曹雪朋),[3] S. P. Hu (胡世鹏),[3] S. H. Yao (姚顺和),[3] and B. B. Yu (于蓓蓓)[3]

[1]*Department of Physics, Tsinghua University, Beijing 100084, People's Republic of China*

[2]*Institute of Modern Physics, Chinese Academy of Sciences, Lanzhou 730000, People's Republic of China*

[3]*China Institute of Atomic Energy, Beijing 102413, People's Republic of China*

(Received 13 May 2012; published 22 June 2012)

Background: ^{139}Pr is located in a transitional region of neutron number close to the $N = 82$ shell. The study of its high-spin states and collective bands is important for systematically understanding the nuclear structural characteristics in this region.

Purpose: To investigate the high-spin levels and to search for oblate bands in ^{139}Pr.

Methods: The high-spin states of ^{139}Pr have been studied via the reaction ^{124}Sn(^{19}F,4n) at a beam energy of 80 MeV. The experiment was carried out at the HI-13 Tandem Accelerator at the China Institute of Atomic Energy (CIAE). The data analysis was done by using the γ-γ coincidence method.

Results: The level scheme of ^{139}Pr has been expanded with spin up to $45/2\hbar$. A total of 39 new levels and 45 new transitions are identified. Four collective band structures at high-spin states have been newly established. From systematic analysis, one of the bands is proposed as a double decoupled band; two bands are proposed as oblate bands with $\gamma \sim -60^\circ$; another band is suggested as an oblate-triaxial band with $\gamma \sim -90^\circ$. The other characteristics for these bands are discussed.

Conclusions: A new level scheme in ^{139}Pr has been established and the collective bands at high spin have been identified. The result shows that the strong oblate shape-driving effect is caused by neutrons at the high-spin states in ^{139}Pr.

DOI: 10.1103/PhysRevC.85.064322 PACS number(s): 21.10.Re, 23.20.Lv, 27.60.+j, 25.70.Jj

I. INTRODUCTION

The study of nuclear high-spin states in the $A = 130$–140 mass region can provide a wealth information about nuclear structures, such as the signature inversion phenomenon in $\pi h_{11/2} \otimes \nu h_{11/2}$ bands of Cs and La isotopes [1,2], the superdeformed bands in Ce, Pr, Nd, Pm, Sm, and Eu isotopes [3–8], and the chiral doublet bands in ^{134}Pr, ^{130}Cs, ^{132}La, ^{136}Pm, and ^{138}Eu nuclei [9–11]. ^{139}Pr with $Z = 59$ and $N = 80$ is located in a transitional region of neutron number close to the $N = 82$ shell. Such nuclei in this region should show small β_2 deformation and soft γ deformation at low spin. Their proton Fermi surface lies at the lower part of the $h_{11/2}$ subshell, while the neutron Fermi surface lies at the upper part of the $h_{11/2}$ subshell. From the cranked shell model (CSM) calculations [12], the alignments of a pair of $h_{11/2}$ protons tend to drive the nucleus towards prolate shape with $\gamma \sim 0^\circ$, whereas the alignments of a pair of $h_{11/2}$ neutrons tend to drive the nucleus towards oblate shape with $\gamma \sim -60^\circ$. Thus, at the high-spin states, the different quasiparticle configurations in a nucleus will give rise to different nuclear shapes. In previous publications, one of important results is the observation of oblate bands caused by such shape driving effects, for instance, in ^{131,136,137}La [2,12,13], ^{132}Ba [14], ^{137,138}Ce [15,16], ^{137,138}Pr [17,18], ^{139}Nd [19], and ^{140,141}Pm [20,21].

For the $N = 80$ isotones in this region, ^{137}La, ^{138}Ce, and ^{141}Pm have been investigated extensively and many oblate bands have been identified [2,16,21]. In ^{139}Pr, the level structures have been established in early reports by using ^{139}La(^{3}He,3n), ^{140}Ce(p,2n), and ^{139}La(α,4n) reactions [22,23], and then were studied by using the ^{130}Te(^{14}N,5n) reaction [24]. However, the high-spin data of ^{139}Pr are rather lacking, and no collective band structure was observed. In this article, we report on new experimental results of high-spin states in ^{139}Pr.

II. EXPERIMENT AND RESULTS

The high-spin states of ^{139}Pr were populated through the heavy-ion fusion-evaporation reaction ^{124}Sn(^{19}F,4n) at a beam energy of 80 MeV. The experiment was carried out using the HI-13 Tandem Accelerator at the China Institute of Atomic Energy (CIAE). The target was an enriched ^{124}Sn of thickness 5.76 mg/cm^2 on a lead substrate with thickness 14.85 mg/cm^2. Twelve Compton-suppressed HPGe detectors and two planar HPGe detectors were employed to detect the in-beam γ rays. Two- and higher-fold coincidence events were recorded. The angles of these detectors with respect to the beam direction were one at 35°, two at 42°, five at 90°, one at 127°, two at 140°, and three at 150°. A total of 5.2×10^7 coincidence events were collected after the subtraction of background. A γ-γ coincidence matrix and an asymmetry two-dimensional angular-correlation matrix were constructed. The asymmetry matrix was produced by the method introduced in Ref. [14]. The coincidence data were analyzed with the RADWARE software package [25].

*zhushj@mail.tsinghua.edu.cn

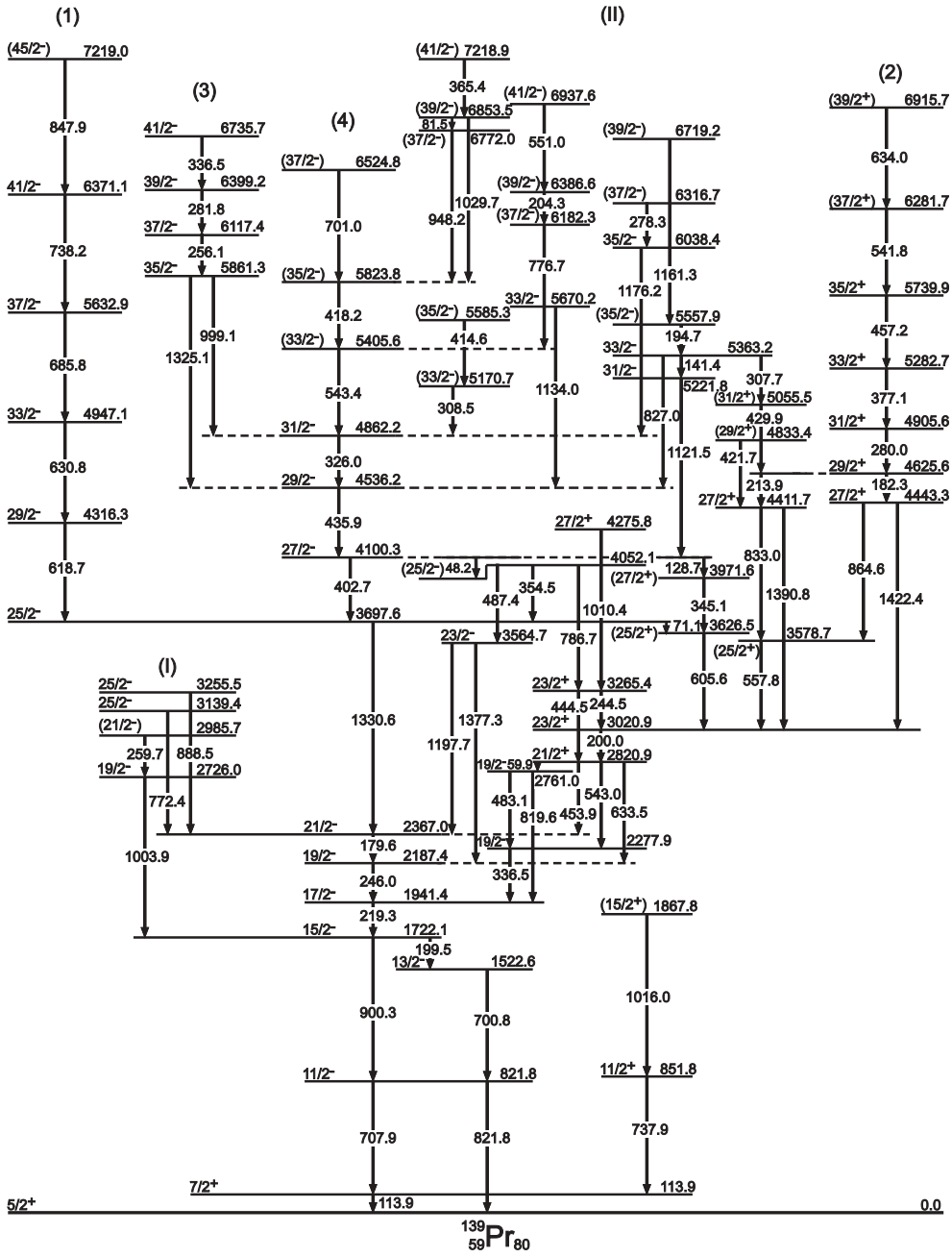

FIG. 1. Level scheme of ^{139}Pr obtained in the present work. Energies are in keV.

After careful data analysis, a level scheme of ^{139}Pr obtained from the present experiment is shown in Fig. 1. Compared to the previous result in Ref. [24], the level scheme of ^{139}Pr has been updated and expanded. Four collective band structures have been newly identified, as labeled by numbers (1)–(4) on the top of the bands in Fig. 1. A total of 39 new levels and 45 new transitions are identified. As examples, Figs. 2 and 3 show the coincidence γ-ray spectra in ^{139}Pr. In Fig. 2, by summing gating on the 707.9 and 900.3 keV γ transitions, all γ transitions in Fig. 1 can be seen clearly except for the γ peaks of 737.9 keV, 1016.0 keV, and those with energy lower than 100 keV. The portion of coincidence spectra observed by gating on 618.7, 1422.4, and 999.1 keV γ transitions is shown in Figs. 3(a), 3(b), and 3(c), respectively. In these figures, the corresponding γ transitions inside bands (1)–(3) can be seen, such as the 630.8, 685.8, 738.2, and 847.9 keV transitions in band (1) [Fig. 3(a)], 182.3, 280.0, 377.1, 457.2, 541.8, and 634.0 keV transitions in band (2) [Fig. 3(b)], and 256.1, 281.8, and 336.5 keV transitions in band (3) [Fig. 3(c)].

Band (1) is newly established based on the 3697.6 keV level and consists of five $\Delta I = 2$ transitions of 618.7, 630.8, 685.8, 738.2, and 847.9 keV. Now we discuss the construction of band (2). In Ref. [24], the 182.3, 213.8, 280.0, and 429.7 keV γ transitions have been observed with the cascade sequence of 182.3 → 429.7 → 213.8 → 280.0 keV which feeds into the

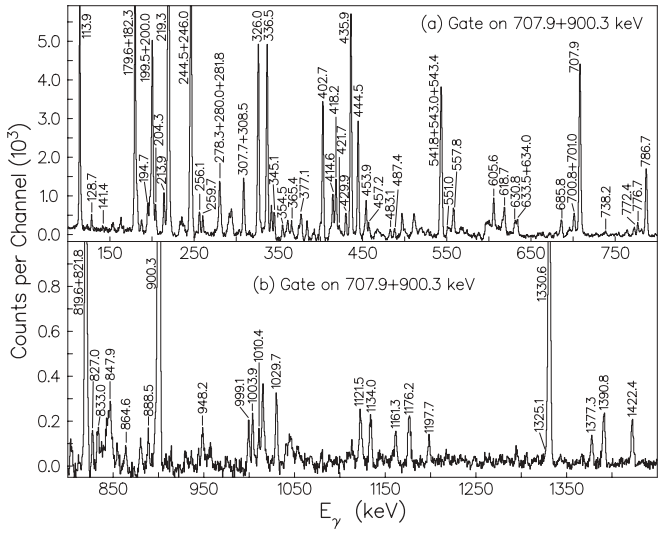

FIG. 2. The coincidence γ-ray spectra by summing gating on 707.9 and 900.3 keV γ transitions in ^{139}Pr. The energy intervals of γ peaks (a) from 100 to 800 keV, and (b) from 800 to 1450 keV.

3020.9 keV level. According to our new data, the cascade sequence of these γ transitions has been rearranged to $280.0 \rightarrow 182.3$ keV and $429.9 \rightarrow 213.9$ keV cascades which feed into the 4443.3 and 4411.7 keV levels, respectively. They finally feed into 3020.9 keV level through 1422.4 and 1390.8 keV γ transitions, respectively. We assigned 182.3 and 280.0 keV γ transitions along with four newly identified γ transitions of 377.1, 457.2, 541.8, and 634.0 keV as band (2). For band (3), the band-head energy is 5861.3 keV. It consists of three $\Delta I = 1$ transitions of 256.1, 281.8, and 336.5 keV and is connected with band (4) through 999.1 and 1325.1 keV γ transitions. For band (4), the γ transitions of 435.9, 326.0, 543.4, and 418.2 keV in this band have been reported in Ref. [24], but they were not assigned as a band structure. We confirmed these γ transitions with present experimental data,

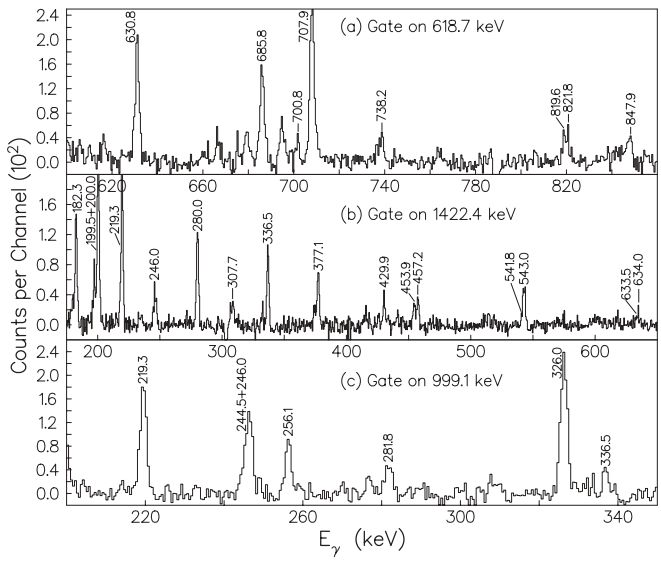

FIG. 3. Portion coincidence γ-ray spectra by gating on (a) 618.7 keV, (b) 1422.4 keV, and (c) 999.1 keV γ transitions in ^{139}Pr.

and identified a new transition of 701.0 keV. According to the regular level spacings, we assigned them as a band structure built on the 4100.3 keV level.

The multipolarities of γ transitions are determined according to the directional correlation of oriented state (DCO) intensity ratio [26]. To obtain the DCO ratio, the asymmetry matrix has been used. Since the statistics of the asymmetry matrix is poorer than that of the total γ-γ coincidence matrix, the DCO ratios of some weak γ peaks cannot be determined. So, the multipolarities of some γ transitions which cannot be determined from the DCO ratios are adopted according to the previous experimental results or deduced from the regular level spacings. Generally, the DCO ratios for $\Delta I = 1$ transitions are around 1.67, while for $\Delta I = 2$ transitions the DCO ratios are around 1.10 from our experiment data. The relative transition intensities are normalized to that of the 707.9 keV transition. The DCO ratios, the multipolarities, and the spin and parity (I^π) assignments of all γ transitions in ^{139}Pr are listed in Table I. In this table, the new transitions have been marked with an asterisk (*) on the transition energies in the first column, and the superscripts a and b in the last column denote the multipolarity taken from Refs. [22] and [24], respectively.

III. DISCUSSION

In the previous study of ^{139}Pr [22], the low-spin states can be interpreted as an odd proton coupled to the excited states of even-even core. In their interpretation, the positive parity states in ^{139}Pr can be obtained by coupling proton $2d_{5/2}$ or $1g_{7/2}$ orbits to the quadrupole vibration of the core, whereas the negative parity states can be obtained by coupling the neutron $1h_{11/2}$ orbit to the quadrupole vibration of the core. Hence, the $5/2^+$ ground state, the $7/2^+$ state at 113.9 keV, and the $11/2^-$ state at 821.8 keV mainly originate from the proton $d_{5/2}$, $g_{7/2}$, and $h_{11/2}$ orbits, respectively. Figure 4 shows a systematic comparison of the low-spin levels of ^{139}Pr with those of the $N = 80$ isotones ^{136}Ba [27], ^{137}La [2], ^{138}Ce [16], ^{140}Nd [28], and ^{141}Pm [21]. The excited states of odd-A ^{137}La, ^{139}Pr, and ^{141}Pm are normalized to the $11/2^-$ states. From Fig. 4, it is shown that the spacings between $11/2^-$ and $15/2^-$ levels in odd-A ^{137}La, ^{139}Pr, and ^{141}Pm are similar to those of the ground bands of even-even core ^{136}Ba, ^{138}Ce, and ^{140}Nd, respectively. In addition, the spacings between $11/2^-$ and $13/2^-$ levels also have similar behavior. Therefore, the $13/2^-$ and $15/2^-$ levels in ^{137}La, ^{139}Pr, and ^{141}Pm are interpreted as a $\pi h_{11/2} \otimes 2^+$ multiplet [22,29]. The $\pi h_{11/2} \otimes 2^+$ multiplet in ^{139}Pr was studied by a triaxial rotor plus particle model in Ref. [22]. The theoretical calculation well reproduces the order of the multiplet levels. Besides, by comparing to ^{141}Pm [30], it is suggested that the $19/2^-$ level at 2187.4 keV in ^{139}Pr may originate from the $\pi h_{11/2} \otimes 4^+$.

To obtain a further understanding for the ground state characteristic of ^{139}Pr, we have carried out the cranked shell model (CSM) calculations [31–33]. The calculation results are presented in Fig. 5, where the minima in the total Routhian surfaces (TRSs) can be found, corresponding to $\beta_2 = 0.088$, $\gamma = -119.948^\circ$ at $\hbar\omega = 0.0$ MeV; $\beta_2 = 0.093$, $\gamma = -4.537^\circ$

TABLE I. The energies, relative intensities, DCO ratios, multipolarities, and spin and parity (I^{π}) assignments of the γ transitions in ^{139}Pr. New transitions have been marked with an asterisk (*) on the transition energies in the first column, and the superscripts a and b in the last column denote the multipolarity taken from Refs. [22] and [24], respectively.

E_{γ} (keV)	Intensities (%)	Assignment	R_{DCO}	Multipolarities
(48.2)		$27/2^{-} \rightarrow (25/2^{-})$		$(M1/E2)$
(59.9)		$21/2^{+} \rightarrow 19/2^{-}$		$(E1)$
(71.1)*		$25/2^{-} \rightarrow (25/2^{+})$		$(E1)$
(81.5)*		$(39/2^{-}) \rightarrow (37/2^{-})$		$(M1/E2)$
113.9	>112.6	$7/2^{+} \rightarrow 5/2^{+}$		$M1^{a}$
128.7	0.16(4)	$27/2^{-} \rightarrow (27/2^{+})$		$(E1)$
141.4*	0.50(11)	$33/2^{-} \rightarrow 31/2^{-}$	1.52(17)	$M1/E2$
179.6	25.0(9)	$21/2^{-} \rightarrow 19/2^{-}$		$M1/E2^{a}$
182.3	0.44(5)	$29/2^{+} \rightarrow 27/2^{+}$	1.64(22)	$M1/E2$
194.7*	0.61(12)	$(35/2^{-}) \rightarrow 33/2^{-}$	1.81(20)	$M1/E2$
199.5	5.2(9)	$15/2^{-} \rightarrow 13/2^{-}$		$M1^{a}$
200.0	2.6(5)	$23/2^{+} \rightarrow 21/2^{+}$		$M1^{a}$
204.3*	0.34(5)	$(39/2^{-}) \rightarrow (37/2^{-})$	1.71(15)	$M1/E2$
213.9	0.46(5)	$29/2^{+} \rightarrow 27/2^{+}$	1.57(12)	$M1/E2$
219.3	62.0(9)	$17/2^{-} \rightarrow 15/2^{-}$		$M1/E2^{a}$
244.5	0.24(5)	$23/2^{+} \rightarrow 23/2^{+}$		$M1/E2^{b}$
246.0	31.2(10)	$19/2^{-} \rightarrow 17/2^{-}$		$M1/E2^{a}$
256.1*	0.39(5)	$37/2^{-} \rightarrow 35/2^{-}$	1.73(8)	$M1/E2$
259.7*	1.4(2)	$(21/2^{-}) \rightarrow 19/2^{-}$	1.56(15)	$M1/E2$
278.3*	0.21(4)	$(37/2^{-}) \rightarrow 35/2^{-}$	1.68(12)	$M1/E2$
280.0	0.65(13)	$31/2^{+} \rightarrow 29/2^{+}$	1.66(20)	$M1/E2$
281.8*	0.32(9)	$39/2^{-} \rightarrow 37/2^{-}$	1.64(8)	$M1/E2$
307.7*	0.25(5)	$33/2^{-} \rightarrow (31/2^{+})$		$(E1)$
308.5*	0.42(6)	$(33/2^{-}) \rightarrow 31/2^{-}$	1.67(9)	$M1/E2$
326.0	6.8(4)	$31/2^{-} \rightarrow 29/2^{-}$	1.59(4)	$M1/E2$
336.5	16.0(8)	$19/2^{-} \rightarrow 17/2^{-}$		$M1^{a}$
336.5*	0.12(2)	$41/2^{-} \rightarrow 39/2^{-}$	1.62(17)	$M1/E2$
345.1	0.37(3)	$(27/2^{+}) \rightarrow (25/2^{+})$	1.82(12)	$M1/E2$
354.5	1.5(2)	$(25/2^{-}) \rightarrow 25/2^{-}$	1.11(11)	$M1/E2$
365.4	0.33(5)	$(41/2^{-}) \rightarrow (39/2^{-})$	1.57(14)	$M1/E2$
377.1*	0.42(6)	$33/2^{+} \rightarrow 31/2^{+}$	1.84(7)	$M1/E2$
402.7	12.9(6)	$27/2^{-} \rightarrow 25/2^{-}$	1.48(5)	$M1/E2$
414.6	0.35(5)	$(35/2^{-}) \rightarrow (33/2^{-})$	1.74(12)	$M1/E2$
418.2	1.31(9)	$(35/2^{-}) \rightarrow (33/2^{-})$	1.70(10)	$M1/E2$
421.7*	0.11(4)	$(29/2^{+}) \rightarrow 27/2^{+}$	1.57(20)	$M1/E2$
429.9	0.3(1)	$(31/2^{+}) \rightarrow 29/2^{+}$	1.69(15)	$M1/E2$
435.9	11.5(4)	$29/2^{-} \rightarrow 27/2^{-}$	1.67(4)	$M1/E2$
444.5	3.6(6)	$23/2^{+} \rightarrow 21/2^{+}$		$M1^{a}$
453.9	2.6(7)	$21/2^{+} \rightarrow 21/2^{-}$		$E1^{b}$
457.2*	0.25(3)	$35/2^{+} \rightarrow 33/2^{+}$	1.58(12)	$M1/E2$
483.1*	0.9(2)	$19/2^{-} \rightarrow 19/2^{-}$		$(M1/E2)$
487.4*	1.2(2)	$(25/2^{-}) \rightarrow 23/2^{-}$	1.79(20)	$M1/E2$
541.8*	0.13(3)	$(37/2^{+}) \rightarrow 35/2^{+}$		$(M1/E2)$
543.0	8.5(12)	$21/2^{+} \rightarrow 19/2^{-}$		$E1^{a}$
543.4	3.3(2)	$(33/2^{-}) \rightarrow 31/2^{-}$		$(M1/E2)$
551.0*	0.20(7)	$(41/2^{-}) \rightarrow (39/2^{-})$	1.72(22)	$M1/E2$
557.8*	0.5(1)	$(25/2^{+}) \rightarrow 23/2^{+}$	1.81(13)	$M1/E2$
605.6	0.5(2)	$(25/2^{+}) \rightarrow 23/2^{+}$	1.87(13)	$M1/E2$
618.7*	2.5(3)	$29/2^{-} \rightarrow 25/2^{-}$	1.03(13)	$E2$
630.8*	0.9(2)	$33/2^{-} \rightarrow 29/2^{-}$	0.96(17)	$E2$
633.5*	1.6(2)	$21/2^{+} \rightarrow 19/2^{-}$	1.47(16)	$E1$
634.0*	<0.1	$(39/2^{+}) \rightarrow (37/2^{+})$		$(M1/E2)$
685.8*	0.7(1)	$37/2^{-} \rightarrow 33/2^{-}$	1.01(7)	$E2$
700.8	5.5(9)	$13/2^{-} \rightarrow 11/2^{-}$		$M1/E2^{a}$

TABLE I. (*Continued*.)

E_γ (keV)	Intensities (%)	Assignment	$R_{\rm DCO}$	Multipolarities
701.0*	<0.1	$(37/2^-) \rightarrow (35/2^-)$		$(M1/E2)$
707.9	100.0(4)	$11/2^- \rightarrow 7/2^+$		$M2^a$
737.9	12.6(2)	$11/2^+ \rightarrow 7/2^+$		$E2^a$
738.2*	0.16(6)	$41/2^- \rightarrow 37/2^-$	1.19(11)	$E2$
772.4*	1.4(2)	$25/2^- \rightarrow 21/2^-$	1.04(10)	$E2$
776.7*	0.51(6)	$(37/2^-) \rightarrow (33/2^-)$	1.06(12)	$E2$
786.7	2.6(5)	$(25/2^-) \rightarrow 23/2^+$	1.76(8)	$E1$
819.6	14.5(9)	$19/2^- \rightarrow 17/2^-$	1.72(7)	$M1/E2$
821.8	4.8(9)	$11/2^- \rightarrow 5/2^+$		$E3^a$
827.0	0.9(2)	$33/2^- \rightarrow 29/2^-$	1.29(14)	$E2$
833.0*	0.19(4)	$27/2^+ \rightarrow (25/2^+)$	1.68(22)	$M1/E2$
847.9*	0.14(5)	$(45/2^-) \rightarrow 41/2^-$		$(E2)$
864.6*	0.10(3)	$27/2^+ \rightarrow (25/2^+)$		$(M1/E2)$
888.5*	0.4(1)	$25/2^- \rightarrow 21/2^-$	0.94(11)	$E2$
900.3	66.3(36)	$15/2^- \rightarrow 11/2^-$		$E2^a$
948.2*	0.32(7)	$(37/2^-) \rightarrow (35/2^-)$	1.71(24)	$M1/E2$
999.1*	0.55(9)	$35/2^- \rightarrow 31/2^-$	1.02(5)	$E2$
1003.9*	1.5(3)	$19/2^- \rightarrow 15/2^-$	1.03(11)	$E2$
1010.4*	0.24(5)	$27/2^+ \rightarrow 23/2^+$	1.25(17)	$E2$
1016.0	12.3(19)	$(15/2^+) \rightarrow 11/2^+$		$E2^a$
1029.7	0.64(9)	$(39/2^-) \rightarrow (35/2^-)$	1.09(11)	$E2$
1121.5*	0.8(2)	$31/2^- \rightarrow 27/2^-$	1.29(14)	$E2$
1134.0*	1.0(2)	$33/2^- \rightarrow 29/2^-$	1.02(10)	$E2$
1161.3*	0.3(1)	$(39/2^-) \rightarrow (35/2^-)$	1.25(20)	$E2$
1176.2	0.8(1)	$35/2^- \rightarrow 31/2^-$	1.19(14)	$E2$
1197.7*	0.5(2)	$23/2^- \rightarrow 21/2^-$	1.63(22)	$M1/E2$
1325.1*	0.10(8)	$35/2^- \rightarrow 29/2^-$		$(M3/E4)$
1330.6	19.2(10)	$25/2^- \rightarrow 21/2^-$	0.98(4)	$E2$
1377.3*	1.2(3)	$23/2^- \rightarrow 19/2^-$	1.08(12)	$E2$
1390.8*	0.5(2)	$27/2^+ \rightarrow 23/2^+$	1.12(10)	$E2$
1422.4*	0.5(2)	$27/2^+ \rightarrow 23/2^+$	1.16(14)	$E2$

at $\hbar\omega = 0.2$ MeV; and $\beta_2 = 0.078$, $\gamma = -119.706^\circ$ at $\hbar\omega = 0.4$ MeV. It is shown that ^{139}Pr has small β_2 deformation and soft γ deformation at the ground state, which agrees with the nuclear characteristics in this region.

As bands (1)–(4) in ^{139}Pr are newly identified in the present work, we discuss the characteristics of these bands in the following paragraphs.

Band (1) consists of $\Delta I = 2$ $E2$ transitions. This band should belong to a double decoupled band which was also observed in the neighboring odd-odd ^{134,136}Pr [9,34], ^{138,140}Pm [20,35], and $N = 80$ odd-A ^{141}Pm [21]. The origin of this band structure is the configuration for a valence neutron or valence proton including a low-Ω orbital, so a large signature splitting between the favored and unfavored constituents occurs [34]. Only one signature constituent is observed in the present work. In Ref. [21], the possible configuration for the double decoupled band in ^{141}Pm was suggested as $\pi h_{11/2} \otimes \nu(h_{11/2} \cdot f_{7/2}[541]1/2^-)$. From the similarity of level characteristics between band (1) in ^{139}Pr and the double decoupled band (1) in ^{141}Pm, we suggested the possible configuration with $\pi h_{11/2} \otimes \nu(h_{11/2} \cdot f_{7/2}[541]1/2^-)$ for band (1) in ^{139}Pr.

Band (2) and band (3) in ^{139}Pr only consist of $\Delta I = 1M1$ transitions inside the bands. Plenty of similar band structures have been observed in this region. These bands were assigned as oblate bands with $\gamma \sim -60^\circ$ which originate from the alignments of a pair of $h_{11/2}$ neutrons [12]. The oblate bands in this region show distinct features [2,12–21]: (a) strong $\Delta I = 1$ transitions relative to the $E2$ crossover transitions, (b) no signature splitting, and (c) moments of inertia different from those of prolate bands.

In the present work, the $E2$ crossover transitions are too weak to be observed and only the $M1$ transitions were observed in bands (2) and (3) in ^{139}Pr. Hence, bands (2) and (3) show the first characteristic of an oblate band. Now we examine the signature splitting feature. Figure 6 shows the plot of the energy staggering parameter $[E(I) - E(I-1)]/2I$ against the spin I for bands (2)–(4) in ^{139}Pr. From this figure, it is shown that the signature splittings of bands (2) and (3) are rather small compared to that of band (4), which is in agreement with the second characteristic of an oblate band. Plots of the moments of inertia $J^{(1)}$ of bands (2)–(4) in ^{139}Pr, oblate bands in ^{131}La [12], ^{137}La [2], and ^{137}Pr [17], and prolate bands in ^{132}Ba [36] and ^{134}Ce [37] against the rotational

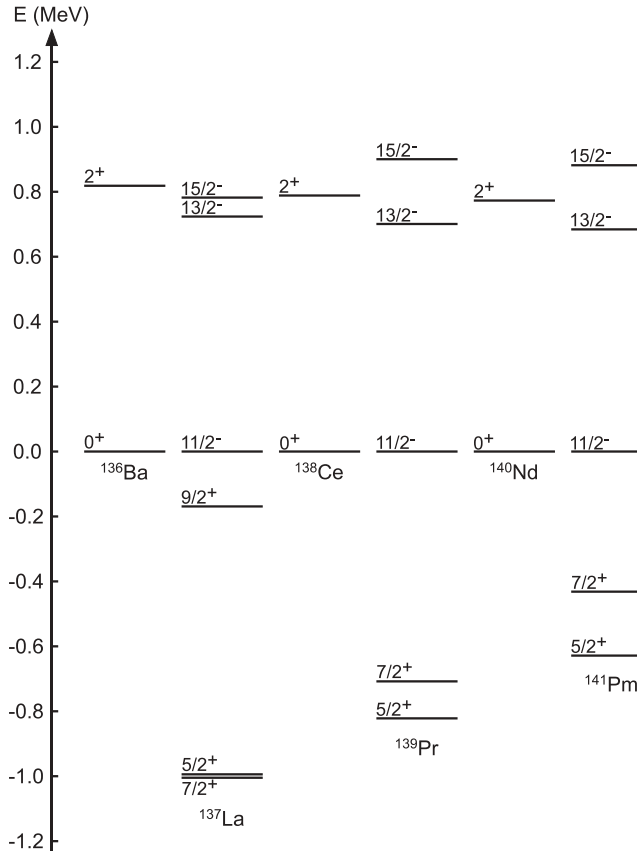

FIG. 4. The systematic comparison of the low-spin levels of ^{139}Pr with the $N = 80$ isotones ^{136}Ba, ^{137}La, ^{138}Ce, ^{140}Nd, and ^{141}Pm.

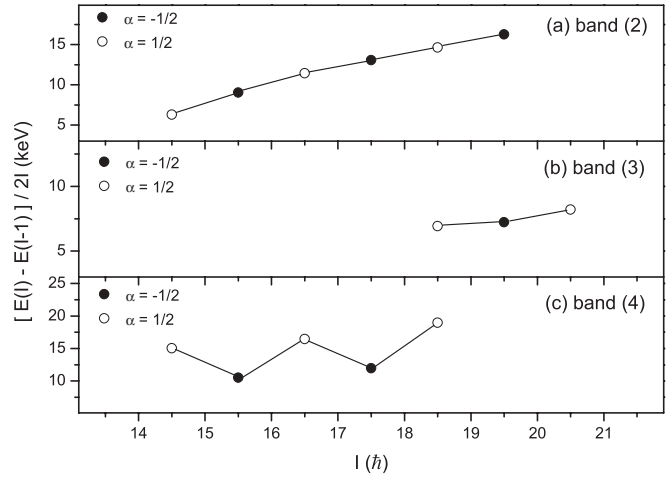

FIG. 6. Plots of the energy staggering parameter $[E(I) - E(I-1)]/2I$ against the spin I for (a) band (2), (b) band (3), and (c) band (4) in ^{139}Pr.

frequency $\hbar\omega$ are presented in Fig. 7. From this figure one can see that the bands (2) and (3) in ^{139}Pr exhibit similar moments of inertia to those of the oblate bands in ^{131}La, ^{137}La, and ^{137}Pr, but different from those of the prolate bands in ^{132}Ba and ^{134}Ce. This coincides with the third characteristic of an oblate band. Thus, the above analysis gives evidences for the oblate band assignments for bands (2) and (3) in ^{139}Pr.

Since the oblate bands originate from the alignments of a pair of $h_{11/2}$ neutrons, the configuration of an oblate band should include a pair of $h_{11/2}$ neutrons. For band (2), the energy of the band-head level is 4443.3 keV. It probably belongs to a three-quasiparticle band. Considering the parity and the orbits around the Fermi surface, we suggest the configuration of band (2) as $\pi g_{7/2} \otimes (\nu h_{11/2})^2$ or $\pi d_{5/2} \otimes (\nu h_{11/2})^2$. For band (3), as its excitation energy is higher than that of band (2), here a five-quasiparticle configuration is suggested. By systematically comparing to the oblate band in ^{137}La [2], we proposed band (3) with a $\pi g_{7/2} d_{5/2} h_{11/2} \otimes (\nu h_{11/2})^2$ configuration.

Band (4) in ^{139}Pr also consists of strong $\Delta I = 1$ $M1$ transitions inside the band, and the moments of inertia are closer to those of the oblate bands rather than those of the

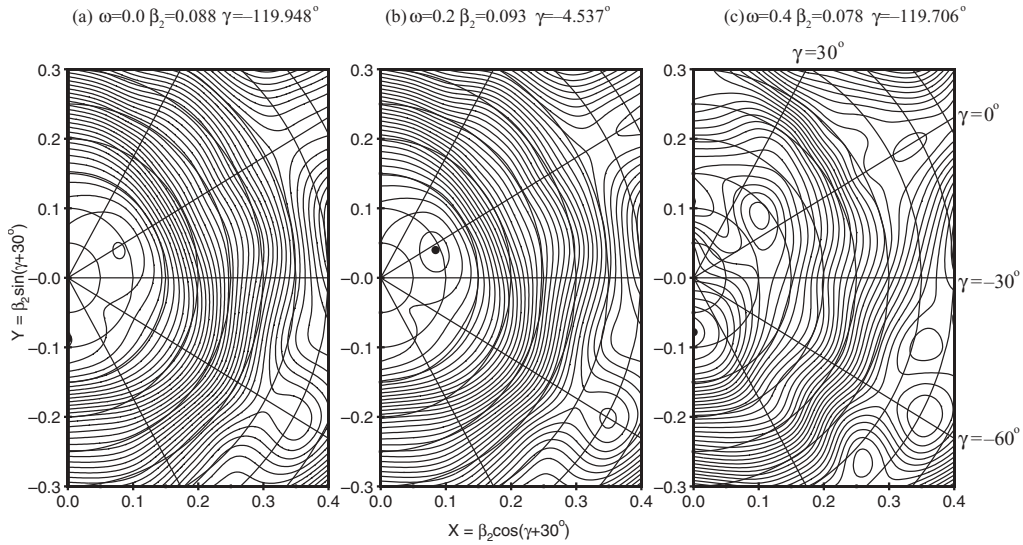

FIG. 5. Polar coordinate plots of total Routhian surface (TRS) calculated for ^{139}Pr at (a) $\hbar\omega = 0.0$ MeV, (b) $\hbar\omega = 0.2$ MeV, and (c) $\hbar\omega = 0.4$ MeV.

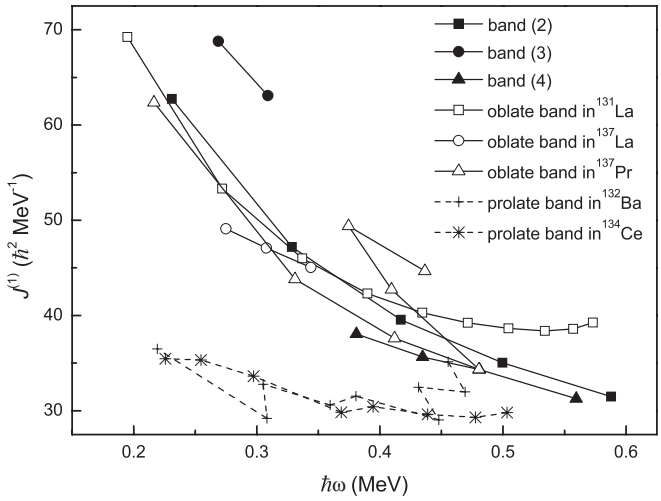

FIG. 7. Plots of the moments of inertia $J^{(1)}$ of bands (2)–(4) in ^{139}Pr, oblate bands in ^{131}La, ^{137}La, and ^{137}Pr, and prolate bands in ^{132}Ba and ^{134}Ce against the rotational frequency $\hbar\omega$.

prolate bands, as shown in Fig. 7. These characteristics show the properties of an oblate band. But as shown in Fig. 6(c), a large signature splitting occurs in this band, which indicates that the band structure is different from an oblate band. This kind of band has been identified in the neighboring nuclei ^{136}Pr [34],^{140}Pm [20], and ^{141}Pm [21], and was suggested as the oblate-triaxial deformation with $\gamma \sim -90^\circ$. Based on the structural similarity, we assigned band (4) in ^{139}Pr as an oblate-triaxial band with $\gamma \sim -90^\circ$ also. In Ref. [34], the oblate-triaxial bands (3) and (7) in ^{136}Pr have been assigned with configurations of $\pi h_{11/2}[505]11/2 \otimes \nu s_{1/2}[400]1/2(h_{11/2})^2$ and $\pi g_{7/2} \otimes \nu s_{1/2}(h_{11/2})^2$, respectively. Based on the structural similarity, we tentatively assigned the configuration of band (4) in ^{139}Pr as $\pi h_{11/2}[505]11/2 \otimes (\nu h_{11/2})^2$.

In Fig. 1, there are many single-particle levels and transitions lying at two sides of low-spin levels and between bands (2) and (4), marked with (I) and (II), respectively. The levels in clusters (I) may belong to three-quasiparticle configurations, and the levels in clusters (II) may have five-quasiparticle configurations according to the excitation energies. These configurations need more theoretical work to be confirmed.

IV. SUMMARY

The high-spin states of ^{139}Pr have been studied in the present work. The level scheme of ^{139}Pr is updated and four collective band structures are established. By systematic comparison and analysis, one band based on the $25/2^-$ state is proposed as a double decoupled band. Two bands based on $27/2^+$ and $35/2^-$ states are suggested as oblate bands with $\gamma \sim -60^\circ$. Another band built on the $27/2^-$ state is suggested as oblate-triaxial deformation with $\gamma \sim -90^\circ$. The possible configurations for these band structures are discussed. It is demonstrated that the strong oblate shape-driving effect is caused by neutrons at the high-spin states in ^{139}Pr.

ACKNOWLEDGMENTS

The work is supported by the National Natural Science Foundation of China under Grants No. 11175095 and No. 10975082, and by the Special Program of Higher Education Science Foundation under Grant No. 2010000211007. The authors thank the staff of the in-beam γ-ray group and the Tandem Accelerator group at the China Institute of Atomic Energy for their warm hospitality during the experiment and for providing the heavy-ion beam and the target.

[1] Y. Liu, J. Lu, Y. Ma, S. Zhou, and H. Zheng, Phys. Rev. C **54**, 719 (1996).
[2] M. L. Li *et al.*, Eur. Phys. J. A **28**, 1 (2006).
[3] J. N. Wilson *et al.*, Phys. Rev. C **55**, 519 (1997).
[4] J. N. Wilson *et al.*, Phys. Rev. Lett. **74**, 1950 (1995).
[5] S. Lunardi *et al.*, Phys. Rev. C **69**, 054302 (2004).
[6] M. A. Riley *et al.*, Phys. Rev. C **47**, R441 (1993).
[7] G. Hackman, S. M. Mullins, J. A. Kuehner, D. Prévost, J. C. Waddington, A. Galindo-Uribarri, V. P. Janzen, D. C. Radford, N. Schmeing, and D. Ward, Phys. Rev. C **47**, R433 (1993).
[8] A. Ataç *et al.*, Phys. Rev. Lett. **70**, 1069 (1993).
[9] C. M. Petrache, D. Bazzacco, S. Lunardi, C. Rossi Alvarez, G. de Angelis, M. De Poli, D. Bucurescu, C. A. Ur, P. B. Semmes, and R. Wyss, Nucl. Phys. A **597**, 106 (1996).
[10] K. Starosta *et al.*, Phys. Rev. Lett. **86**, 971 (2001).
[11] A. A. Hecht *et al.*, Phys. Rev. C **63**, 051302(R) (2001).
[12] E. S. Paul, C. W. Beausang, D. B. Fossan, R. Ma, W. F. Piel, N. Xu, L. Hildingsson, and G. A. Leander, Phys. Rev. Lett. **58**, 984 (1987).
[13] S. J. Zhu, S. D. Xiao, X. L. Che, Y. N. U, M. L. Li, Y. J. Chen, L. H. Zhu, G. S. Li, S. X. Wen, and X. G. Wu, Eur. Phys. J. A **24**, 199 (2005).
[14] E. S. Paul, D. B. Fossan, Y. Liang, R. Ma, and N. Xu, Phys. Rev. C **40**, 1255 (1989).
[15] S. J. Zhu *et al.*, Phys. Rev. C **62**, 044310 (2000).
[16] S. J. Zhu *et al.*, Chin. Phys. Lett. **16**, 635 (1999).
[17] N. Xu, C. W. Beausang, R. Ma, E. S. Paul, W. F. Piel, D. B. Fossan, and L. Hildingsson, Phys. Rev. C **39**, 1799 (1989).
[18] M. L. Li *et al.*, Phys. Rev. C **75**, 034304 (2007).
[19] Q. Xu *et al.*, Phys. Rev. C **78**, 034310 (2008).
[20] J. G. Wang *et al.*, J. Phys. G: Nucl. Part. Phys. **37**, 125107 (2010).
[21] L. Gu *et al.*, Phys. Rev. C **83**, 064303 (2011).
[22] M. Piiparinen, M. Kortelahti, A. Pakkanen, T. Komppa, and R. Komu, Nucl. Phys. A **342**, 57 (1980).
[23] R. Aryaeinejad and Wm C. McHarris, Phys. Rev. C **37**, 1855 (1988).
[24] S. Chanda, S. Bhattacharyya, T. Bhattacharjee, S. S. Ghugre, S. K. Basu, S. Muralithar, R. P. Singh, B. Mukherjee, R. K. Bhowmik, and S. N. Ray, Pramana-J. Phys. **57**, 175 (2001).

[25] D. C. Radford, Nucl. Instrum. Methods Phys. Res., Sect. A **361**, 297 (1995).
[26] K. S. Krane, R. M. Steffen, and R. M. Wheeler, Nucl. Data Tables **11**, 351 (1973).
[27] J. J. Valiente-Dobón *et al*., Phys. Rev. C **69**, 024316 (2004).
[28] A. Neußer *et al*., Phys. Rev. C **70**, 064315 (2004).
[29] M. Kortelahti, A. Pakkanen, M. Piiparinen, T. Komppa, and R. Komu, Nucl. Phys. A **376**, 1 (1982).
[30] S. Bhattacharyya, S. Chanda, T. Bhattacharjee, S. K. Basu, R. K. Bhowmik, S. Muralithar, R. P. Singh, and S. S. Ghugre, Nucl. Phys. A **730**, 23 (2004).
[31] S. Frauendorf, Phys. Lett. B **100**, 219 (1981).
[32] S. Frauendorf and F. R. May, Phys. Lett. B **125**, 245 (1983).
[33] F. R. Xu, W. Satula, and R. Wyss, Nucl. Phys. A **669**, 119 (2000).
[34] C. M. Petrache *et al*., Nucl. Phys. A **603**, 50 (1996).
[35] C. W. Beausang, P. K. Weng, R. Ma, E. S. Paul, W. F. Piel, N. Xu, and D. B. Fossan, Phys. Rev. C **42**, 541 (1990).
[36] S. Juutinen *et al*., Phys. Rev. C **52**, 2946 (1995).
[37] S. J. Zhu, C. Y. Gan, L. Y. Zhu, M. Sakhaee, L. M. Yang, G. L. Long, S. X. Wen, X. G. Wu, G. S. Li, and L. H. Zhu, High Energy Phys. Nucl. Phys. **29**, 130 (2005) (in Chinese).